Blotting Analysis of Native IRP1: A Novel Approach to Distinguish the Different Forms of IRP1 in Cells and Tissues[†]

Alessandro Campanella,[‡] Sonia Levi,[‡] Gaetano Cairo,[§] Giorgio Biasiotto,[#] and Paolo Arosio*[,#]

Dibit, Department of Biological and Technological Research, IRCCS H. San Raffaele, Milano, Italy, Institute of General Pathology, University of Milan, Milan, Italy, and Section of Chemistry, Faculty of Medicine, University of Brescia, Brescia 25125 Italy

Received August 5, 2003; Revised Manuscript Received September 26, 2003

ABSTRACT: Iron regulatory protein 1 (IRP1) is a bifunctional protein, which either has aconitase activity or binds to specific mRNA structures to regulate the expression of iron proteins. Using recombinant human IRP1, we found that the two functional forms are resolved by nondenaturing polyacrylamide gel electrophoresis and that they are distinguished from IRP1/RNA complexes. This allowed us to use specific antibodies to develop a blotting system that recognized the iron-free and iron-containing IRP1 forms in the soluble fraction and the RNA-bound IRP1 in the high-speed precipitate fraction of cell extracts. The system was used to study IRP1 in HeLa, K562 cells, and monocytes/macrophages before and after treatment with iron salts, iron chelators, or hydrogen peroxide, as well as in stomach and duodenum biopsies. The results showed that iron-bound aconitase IRP1 is by far the prevalent form in most cells and that the major effect of cellular iron modifications is a shift between free and RNA-bound IRP1. The fraction of RNA-bound IRP1 was highly variable among different cells and was often a minor one. Furthermore, blotting showed that electrophoretic mobility shift assay, as commonly used, tends to under-evaluate the amount of total IRP1 and to over-evaluate the actual RNA-binding activity of IRP1. In conclusion, blotting analysis of IRP1 is a new, useful, and convenient method to analyze the amount and conformations of the protein that reveals previously undetected differences in IRP1 compartmentalization among various cell types.

Iron regulatory proteins (IRPs)[1] are cytosolic transregulators that maintain iron homeostasis by high affinity binding to iron responsive elements (IRE) in the untranslated regions of the mRNAs for proteins involved in iron metabolism. Although several conditions related to cellular redox status modify IRPs activity (see refs *1*−*4* for recent reviews), binding activity is mainly modulated by cellular iron availability and reflects the iron level of the so-called labile iron pool. In consideration of the increasingly recognized importance of potentially toxic excess "free" iron in a number of pathophysiologic settings, analysis of IRP activity to monitor cellular iron availability may become an important tool to investigate the iron status not only in conditions of iron deficiency or overload but also in other disease states, such as inflammation, malignant growth, and oxidative damage, in which iron is involved. The two mammalian IRPs, IRP1 and IRP2, bind mRNA with similar affinity but respond to cellular stimuli in different ways: IRP2 is regulated through protein stability, while IRP1 switches between an apo/RNA-binding form and a [4Fe-4S] cluster form, without evident changes in protein levels. The [4Fe-4S] form has enzymatic activity and corresponds to the cytosolic aconitase (*5*, *6*). The two activities of IRP1 are mutually exclusive since they use the same structural region located in a pocket between domain 4 and domains 1−3 (*7*, *8*). The switch between the two forms is driven by the assembly/destruction of the [4Fe-4S] cluster. In the cell, the relative abundance of the two forms is related to iron availability: when the metal is abundant the iron-containing aconitase form is prevalent, while in iron deficiency the apo/RNA-binding form is predominant. Also, oxidative stress and hypoxia modify the equilibrium between the two forms with mechanisms that may involve cellular iron deprivation or the attack of reactive molecules directly on the Fe−S clusters (*9*, *10*). The relative proportion of the two main conformations in the cell is usually monitored in an indirect way by electrophoretic mobility shift assays (EMSA) using a radiolabeled IRE probe. The intensity of the autoradiographic band of the complex gives an indication of the "spontaneous" IRE-binding activity (IRE-BP) of the sample, while the total amount of IRP1 is usually estimated by assaying the binding activity of the sample after in vitro treatment with reductants such as 2-mercaptoethanol (2ME) (*11*, *12*). The complexes between IRE and murine IRP1 and IRP2 are easily distinguished

[†] The work was partially supported by Italian National Council of Research (CNR) targeted project to PA, CNR-Agenzia 2000 to P.A. and S.L., and by Italian Ministry of the University and Research (MIUR), Cofin-2001, Cofin-2002 to P.A. and G.C. and Associazione Italiana Ricerca Cancro to G.C.

* Corresponding author: Prof. Paolo Arosio, Department MITB, Viale Europa 11, 25125 Brescia, Italy. Tel: +39-030 394386. Fax: +39-030-307251. E-mail: arosio@med.unibs.it.

[‡] Dibit, Department of Biological and Technological Research, IRCCS H. San Raffaele.

[§] University of Milan.

[#] University of Brescia.

[1] Abbreviations: IRP1: iron regulatory protein 1; rIRP1: recombinant IRP1; IRP2: iron regulatory protein 2; EMSA: electrophoretic mobility shift assay; IRE-BP: IRE binding activity, IRE: iron responsive element; 2ME: 2-mercaptoethanol; PAGE: polyacrylamide gel electrophoresis; DTT: dithiothreitol.

10.1021/bi035386f CCC: $27.50
Published on Web 12/13/2003

because of their different mobilities, while the human ones comigrate and their identification relies on supershift with specific antibodies (*13*). The evaluation of cytosolic aconitase activity is an alternative assay to monitor the conformational status of IRP1, and its increase is always accompanied by a decrease in the IRE-BP activity of IRP1 in the cell (*14*). However, IRP1 may acquire conformations that have neither IRE-BP nor aconitase activity, such as the one with a [3Fe-4S] cluster, and are therefore undetectable (*15*). Also the RNA-bound IRP1, which is the form active in regulating protein expression, is not detectable with either assay. This fraction has been analyzed in mouse fibroblasts by dissociating IRP1 from the polysomal fraction with high salt and testing its activity by EMSA, and it was found to range from undetectable up to more than 14%, in conditions of high and low iron availability, respectively (*16*).

The two major IRP1 conformations are stable in vitro. Human IRP1 expressed in *Escherichia coli* was recovered both in the apo-form with IRE-BP activity (*17*, *18*) or in the aconitase form, depending upon the purification procedure (*19*, *20*). The IRE-BP form is converted to aconitase by incubation with ferrous salts and thiol groups (*17*, *18*), and the aconitase form is converted into the apo-form with IRE-BP activity by reduction with thiolic agents (*19*, *20*). The apo-form was found to be more sensitive to limited proteolysis than the aconitase, an indication that the two have different structural conformations (*21*, *22*). This was supported by small-angle neutron scattering measurements that showed that apo-IRP1 has a larger radius of gyration than aconitase (*19*). This suggested that the two forms might be separated by simple biochemical methods.

Present analysis of recombinant human IRP1 (rIRP1) on nondenaturing PAGE confirmed that the iron-free, iron-bound IRP1, and IRE/IRP1 complex have distinct mobilities. To analyze the different IRP1 forms in cell extracts, we developed a blotting system based on specific antibodies that recognized the IRP1 conformations in the soluble fraction of cell extracts and the RNA-bound form in the precipitate fraction. The assay showed that in untreated HeLa, K562 cells and in extracts from stomach and duodenum biopsies the aconitase form is largely prevalent, while human monocytes/macrophages contained also a substantial amount of iron-free IRP1. The iron-free and the RNA-bound forms increased after iron chelation and decreased after iron supplementation, but the relative amounts of the various forms and the response to iron differed in the three cell types examined. Blotting is a new, useful, and convenient method to analyze the amount and conformations of IRP1 in cell extracts.

EXPERIMENTAL PROCEDURES

Recombinant IRP1. The plasmid pT7-His-hIRF encoding the full-length human IRP1 sequence fused at the N terminus to His_6 tag was kindly provided by Dr. Lukas C. Kuhn. *E. coli* BL21 DE3 were transformed with the plasmid and used for protein expression. This was obtained by growing the cells for 18 h at 25 °C in LB broth without induction. IRP1 was recovered in the soluble fraction of the cell homogenate. The protein was purified using Ni nitrilotriacetic acid-agarose as described in ref *17*, eluted with 100 mM imidazole and dialyzed versus 20 mM Tris-HCl pH 8.0, 15 mM K acetate, 0.15 mM $MgCl_2$, 7.2 mM 2ME, and 5% glycerol. The sample was then applied to a 5 mL ionic exchange HiTrap Q column (Pharmacia) and eluted with a linear gradient of KCl. The purified protein was dialyzed in 20 mM Tris-HCl pH 7.4 and stored at −80 °C. To elicit antibodies, the unreduced purified rRP1 (50 μg) was mixed with adjuvant, and injected in BALB/C mice. After booster injections, the mice were sacrificed and sera collected for analysis by Western blotting. The positive sera were pooled and stored.

Reconstitution of Aconitase Activity. The reconstitution of aconitase activity of rIRP1 was carried out essentially as described in ref *18*. Briefly, 10 μg of purified rIRP1 was aerobically incubated in 150 mM potassium acetate, 1.4 $MgCl_2$, 70 mM DTT, 10% glycerol, 0.8 mM Na_2S, 350 μM Fe-citrate, or 350 μM [^{55}Fe]-citrate (Fe/citrate 4:1) (ICN) for 25 min at 25 °C.

Cell Culture. HeLa cells were grown in DMEM (Life Technologies) supplemented with 10% fetal bovine serum (Clontech), 100 units/mL penicillin, 100 μg/mL streptomycin, and 1 mM L-glutamine. K562 cells were grown in RPMI (Life Technologies) supplemented with 10% fetal bovine serum (Life Technologies), 100 units/mL penicillin, 100 μg/mL streptomycin, and 1 mM L-glutamine. Monocytes were purified as already described (*23*) from buffy coats of healthy blood donors who gave written informed consent. Mononuclear cells were separated by successive density gradient centrifugations on Ficoll-Paque and Percoll solutions. For culturing, monocytes were resuspended in RPMI 1640 medium containing 2 mM L-glutamine, antibiotics, and 20% heat-inactivated human serum and kept in 5% CO_2 at 37 °C (*23*). Medium and all reagents were endotoxin-free. To induce differentiation to macrophages, monocytes were maintained in culture for 7 days. For experiments involving manipulations of iron availability, the cells were grown for 18 h in the medium added of 300 μM ferric ammonium citrate (FAC) or 100 μM desferrioxamine (DFO). In other experiments, cells were exposed for 30 min to 600 μM H_2O_2 in complete medium.

Cellular Extracts. Cells were harvested and homogenized manually with a Teflon potter in 20 mM Tris-HCl pH 7.4, 250 mM sucrose in the presence of 0.007% digitonin. The extracts were first centrifuged at low speed (1500*g*, 10 min) to remove nuclei and cell debris, and the supernatants were centrifuged at 10000*g* for 10 min to remove membranes and obtain cytosolic preparations. This fraction was further centrifuged at 100000*g* for 60 min and the supernatant was referred to as soluble cytosolic preparations. The pellets from the 10000*g* and 100000*g* centrifugation were mixed and resuspended in 20 mM Tris-HCl pH 7.4, 250 mM sucrose, 1% Triton X-100 (Merck). These samples were referred to as cytosolic precipitates. Biopsy specimens were taken from normal appearing mucosa of stomach and duodenum during routine gastroduodenoscopic examination of control subjects who gave written informed consent. The samples were snap frozen and subsequently homogenized with the same procedure used for the cultured cells. Protein concentration was determined using the BCA assay (Pierce) calibrated on bovine serum albumin.

Western Blotting. Samples containing protein extracts from the various subcellular fractions or rIRP1 were separated on nondenaturing 7.5% polyacrylamide gel electrophoresis in Tris-glycine buffer or in nondenaturing 6% polyacrylamide

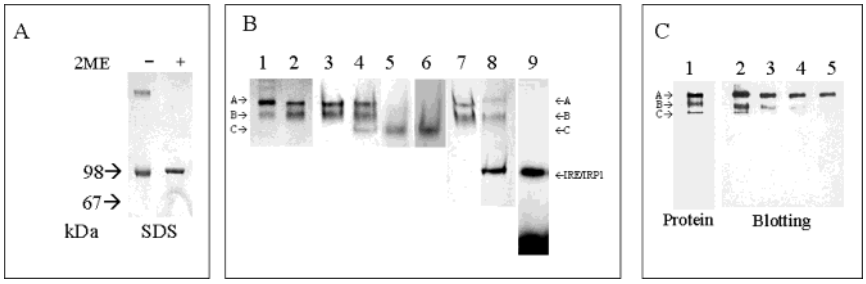

FIGURE 1: Analysis of purified recombinant IRP1. (A) rIRP1 (1 μg) analysis on denaturing 6% SDS−PAGE, before or after 10-min incubation with 2% 2ME. Coomassie blue staining, the migration of molecular weight markers is indicated. (B) rIRP1 (3 μg) analysis on nondenaturing 7.5% PAGE under different conditions: lane 1: untreated sample, lane 2: after 10-min incubation with 2% 2ME, lane 3: after 25-min incubation with 70 mM DTT, lane 4: after 25-min incubation with 70 mM DTT, 0.8 mM Na_2S, 350 μM Fe-citrate and stained with Coomassie blue, lane 5: incubated in the same conditions as lane 4 but using 350 μM [^{55}Fe]-citrate, and the gel exposed to autoradiography, lane 6: as in lane 4 but the gel was overlaid with agarose containing 20 mM $MgCl_2$, 2.5 mM cis-aconitate, 0.25 mM β-NADP, 5 U of isocitric dehydrogenase, 0.6 mM MTT, and 0.3 mM phenazine methosulfate for in situ visualization of aconitase activity; lane 7: rIRP1 in 20 mM Tris-HCl pH 7.4, 70 mM DTT, lane 8: as in lane 7 but after 10-min incubation with unlabeled IRE probe at a molar ratio of 10:1 followed by ribonuclease T1 digestion; the gel was stained with Coomassie blue. Lane 9: 50 ng of rIRP1 were incubated with 100 000 cpm of ^{32}P-labeled IRE probe and the gel exposed to autoradiography. (C) rIRP1 was treated with Fe and sulfide and separated on nondenaturing PAGE as in panel B. Lane 1: Coomassie blue stain of 3 μg of load sample, lanes 2−5: blotting of 5 ng of sample overlaid with decreasing dilutions of anti-IRP1 antiserum (1/750, 1/1500, 1/3000, and 1/4500, respectively) and exposed to ECL development. The three forms of IRP1 were recognized by the antibody with similar affinity because the relative proportion of A, B, and C bands in lane 1 (5.3, 2.9, and 1.0, respectively) was very similar to that of lane 2 (4.9, 3.0, and 1.0, respectively) and because at suboptimal antibody dilution (lanes 3−5) the intensity of the three bands decreased in parallel. The arrows point to the A, B, C bands and the IRE/IRP1 complex. The experiments were performed at least three times, and representative gels are shown.

gel in TBE buffer. Proteins were transferred with a semidry blotting apparatus to Hybond ECL nitrocellulose membranes (Amersham), which were incubated with mouse antiserum anti-IRP1 diluted 1:750 and with secondary, peroxidase labeled anti mouse Ig diluted 1:4000 (Sigma). Bound activity was revealed with Super Signal West Pico system (Pierce). Band intensity of the exposed films was quantified by gel densitometry and the area of each band was subtracted of background. Linearity was assessed by the linear increase of band density with protein load. All data refer to a comparison of band intensity within the same film exposure.

Electro Mobility Shift Assay. The IRE probe was generated by in vitro transcription of the plasmid pSPT-fer (*24*). The plasmid was linearized with BamHI and transcribed by T7 RNA polymerase in the presence of 80 μCi [^{32}P]UTP (ICN) or with 0.4 mM UTP for labeled and unlabeled probes, respectively. EMSA assays were performed as described in refs *11* and *12*. In brief, cell extracts (2 μg of total protein) were incubated with a molar excess (100 000 cpm) of ^{32}P-labeled IRE probe in the presence or the absence of 1 mM DTT. The samples were run on nondenaturing 6% polyacrylamide PAGE in TBE buffer, and exposed to autoradiography. To distinguish between IRP1 and IRP2, antibody supershift experiments were performed essentially as described in ref *13* with slight modifications. Briefly, specific antibodies for human IRP1 (see above) and for IRP2 (a polyclonal antibody raised in rabbits against a conserved sequence in the degradation domain of IRP2) diluted 25- and 10-fold, respectively, were added to the samples and incubated for 15 min at 25 °C before the addition of the IRE probe.

Aconitase Activity. The aconitase activity in the cellular homogenates was measured spectrophotometrically at 240 nm at 37 °C as described in ref *14* by following the disappearance of cis-aconitate (Sigma). To monitor aconitase activity directly on the nondenaturing PAGE, a 25 mL solution containing 120 mM Tris-HCl pH 8.0, 40 mM $MgCl_2$, 5 mM *cis*-aconitate, 0.5 mM β-NADP, 5 U of isocitric dehydrogenase, 1.2 mM MTT, and 0.6 mM phenazine methosulfate (Sigma) was mixed with an equal volume of 2% agarose in 200 mM Tris-HCl pH 8.0 maintained at 42−43 °C. The mixture was immediately poured to cover the gel and incubated at 37 °C until development of violet stain (*25*).

RESULTS

Immunoblotting Analysis of Recombinant IRP1. Purified recombinant human IRP1 (rIRP1) was composed of a single peptide of the expected size of ∼98 kDa (Figure 1A). Nondenaturing PAGE showed that rIRP1 was resolved into a minor B band and a major A. Band A was partially shifted to B band after reduction with 2% 2-mercaptoethanol (2ME), (Figure 1B, lanes 1 and 2). The protein did not show detectable aconitase activity; however, incubation of rIRP1 with sulfide and iron salts under aerobic conditions (*18*) resulted in the formation of some aconitase activity (specific activity 16−20 U/mg) and the appearance of a new C band running ahead of the B band (Figure 1B, lanes 3 and 4). The C band was the only one showing aconitase activity by direct enzymatic staining of the gel (Figure 1B, lane 6) and the only one associated with iron after reconstitution experiments with ^{55}Fe (Figure 1B, lane 5). We concluded that the C band represents aconitase−IRP1. EMSA with radiolabeled IRE probe showed that rIRP1 and IRP1 present in HeLa cell extracts formed IRE/IRPs complexes with the same electrophoretic mobilities (not shown). Recombinant IRP1 previously treated with a reducing agent was incubated with unlabeled IRE probe and separated on nondenaturing PAGE. Protein stain showed the appearance of a new fast running band with the same mobility as the ^{32}P-labeled IRE/rIRP1 complex (Figure 1B, lanes 8 and 9). The formation of the complex was associated with a decrease of both A and B bands, indicating that they possess similar IRE-BP activity. However, about ∼30% of each band remained unshifted despite the 10-fold molar excess of IRE probe (Figure 1B, lanes 7 and 8).

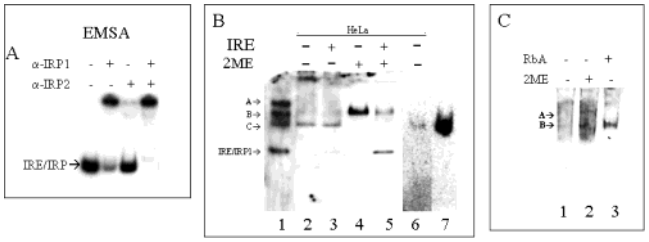

FIGURE 2: Analysis of IRP1 in HeLa cells. The soluble cytosolic fractions of HeLa cell homogenates, in the supernatant after 100000*g* centrifugation, were analyzed by nondenaturing PAGE under different conditions. (A) EMSA of the sample incubated with saturating amounts of antibodies specific for IRP1 (αIRP1), IRP2 (αIRP2) either alone or in combination before addition of the radiolabeled IRE-probe, as indicated. Gels were exposed to autoradiography. (B) Samples of 10 μg of HeLa cell cytosolic fractions were loaded untreated, incubated with 2% 2ME, with 0.5 μL of unlabeled IRE probe or both, as indicated, and separated on nondenaturing 7.5% PAGE. Part of the gel was blotted with anti-rIRP1 (lanes 1−5), as in Figure 1C, and part was stained for aconitase activity (lanes 6 and 7), as in Figure 1B. Samples of rIRP1 were used as control for the localization of the A, B, C bands and for aconitase activity (lanes 1 and 7). (C) IRP1 blotting of cytosolic precipitate from untreated control cells before and after incubation for 10 min with 2% 2ME or for 30 min with 2 μg of ribonuclease A (RbA) at 25 °C. Data are representative of three independent experiments with similar results.

Mouse antisera elicited against rIRP1 proved to be specific for rIRP1 without cross-reactivity with mitochondrial aconitase or IRP2 (not shown) and thus suitable for the recognition of IRP1 in blotting. This was tested by analyzing samples that contained the A, B, and C bands. Figure 1C shows that all the three bands were recognized by the antibody at the optimized dilution 1:750 down to a total load of 5 ng of purified IRP1 (lane 2) and that the ratio of band intensity in the blotting was analogous to that of the corresponding protein stain. The signal of the three bands decreased in parallel with antibody dilution (lanes 3−5) indicating similar affinity binding. The relative proportion of the intensity of three bands did not vary with protein load in the range tested of 5−20 ng (not shown). In contrast, the antibody showed lower affinity for the IRE−IRP1 complex, possibly because some epitopes are masked by RNA.

Analysis of HeLa Cell Soluble Extracts. The recombinant and natural IRP1 are expected to have similar electrophoretic mobility since the histidine tag specific to the recombinant protein has a neutral charge at the pH of the separation and it modifies only slightly the calculated molecular size (99.222 and 98.399 kDa, respectively) and isoelectric point (6.40 and 6.23, respectively). Thus, we used rIRP1 as a reference to identify the various conformations of IRP1 in HeLa cells. The cytosolic extracts were centrifuged at high speed (100000*g*) to remove polysomes and IRP1−mRNA complexes leaving only free IRP1 in a compartment that we named the soluble fraction. The relative content of IRP1 in HeLa cells is unknown, since EMSA does not distinguish human IRP1 and IRP2. To detect it, the fractions were incubated with saturating amounts of antibody against IRP1, which supershifted most of the signal. Incubation with antibody against IRP2 supershifted a lower amount of it, and incubation with the two antibodies together supershifted the signal completely (Figure 2A). Gel densitometry showed a ratio IRP1/IRP2 of about 3:1.

Immunoblotting of the soluble fraction showed that the C band was the major IRP1 component (Figure 2B, lane 2), and in situ enzymatic staining confirmed that the C band had aconitase activity (Figure 2B, lane 6). A faint B band was also visible, while the A band was undetectable. A minor band corresponding to the IRE/IRP1 complex appeared after incubation with the unlabeled IRE probe (Figure 2B, lane 3). Treatment with 2% 2ME resulted in a strong increase of the B form, and disappearance of the C band (Figure 2B, lane 4). Addition of unlabeled IRE probe to the reduced sample shifted most of the B band to the IRE/IRP1 complex leaving about 30% unshifted B band (Figure 2B, lane 5). The incomplete shifting is more likely caused by lack of binding than by dissociation during in vitro handling, since the IRE/IRP1 complex is stable in the conditions used (not shown). The results confirmed the specificity of the antibody and showed that blotting recognizes natural IRP1 apo-, aconitase, and IRE-bound conformers.

Next, we analyzed the 100000*g* precipitate fraction of cell extracts. EMSA detected traces of IRE-BP activity only after incubation with 2% 2ME, while aconitase activity was undetectable (not shown). Blotting showed only smears and no evident IRP1 in the fraction either untreated, incubated with 2% 2ME (Figure 2C, lanes 1 and 2) or with RNase T1 (not shown). However, after a 30-min incubation with 2 μg of RNase-A a component corresponding to the B band became visible (Figure 2C, lane 3). This finding is consistent with the hypothesis that in this fraction most IRP1 is RNA-bound and therefore cannot migrate in the gel and/or be transferred to the membrane, but it can be released from the complex by RNase-A digestion. The same RNase-A treatment caused the disappearance of the in vitro formed rIRP1−IRE complex (not shown) confirming the hypothesis that the bound RNA is susceptible to enzymatic digestion.

All together, the data show that all soluble IRP1 can be detected after 2% ME treatment of the soluble extract, and that the RNA-bound IRP1 can be detected after RNase-A treatment of the precipitated cellular fraction. Thus, blotting permits one to verify the movements of IRP1 between the two major functional compartments (free and RNA-bound) under different cellular conditions. In addition, it permits detection of the iron-free and iron-bound forms of free IRP1.

IRP1 Modifications in HeLa Cells. Having demonstrated that treatment of the soluble and precipitate fractions with reductants and RNase-A, respectively, allows reliable quantification of all IRP1, we analyzed HeLa cells subjected to iron supplementation or chelation by exposure for 18 h to 300 μM FAC or 100 μM DFO, respectively, or subjected to oxidative stress by a 30-min incubation with 600 μM H_2O_2. Gel densitometry of the blots showed that the amount of total IRP1 in the soluble cellular fraction slightly increased ∼10% after iron supplementation and decreased ∼40−50% after DFO or H_2O_2 treatments (Figure 3). These modifications seemed to be caused by the formation of complexes with RNA, since IRP1 in the precipitate fraction decreased ∼70% in the iron supplemented cells, increased in the H_2O_2-treated cells (∼2-fold) and even more in the DFO-treated cells (∼3-fold). These results show that the IRP1 modifications in the soluble and precipitated fractions following the various treatments are complementary, leaving the total amount of cellular IRP1 essentially unaffected. Next we analyzed IRP1 conformers in the soluble fraction of the extracts. DFO

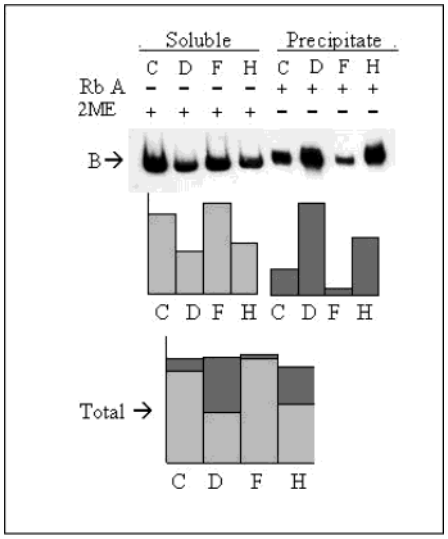

FIGURE 3: IRP1 in the soluble and precipitate fraction of HeLa cells after iron chelation, supplementation, or H_2O_2 treatment. HeLa cells were grown for 18 h in the presence of 100 μM desferroxamine (D), 300 μM ferric ammonium citrate (F), or incubated for 30 min with 600 μM H_2O_2 (H) or left untreated (C). Then they were harvested and the soluble cytosolic and precipitate fractions were prepared as described in Materials and Methods. The soluble fraction was incubated with 2% 2ME and the precipitate with RNase-A as in Figure 2. Samples of 10 μg of total proteins were analyzed on nondenaturing 6% PAGE and blotted with anti-IRP1 antibody. The histogram under the electrophoretic patterns shows the densitometric values of the bands. Signals from the two fractions were directly compared: the lower histogram shows the relative amount of IRP1 in the two fractions, and it was obtained by adding the densitometric values of the soluble (lighter bar) and precipitate fraction (darker bar) after correction for the protein content of each fraction. Data are representative of three independent experiments with similar results.

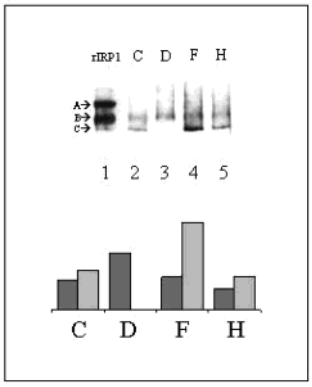

FIGURE 4: IRP1 conformations in the soluble extracts of HeLa cells after iron chelation, supplementation, or H_2O_2 treatment. HeLa cells were treated as in Figure 3. Samples of soluble extracts (10 μg) were analyzed on nondenaturing 7.5% PAGE and blotted with anti-IRP1 antibody. The arrows indicate the position of the A, B, and C bands. The histograms of gel densitometry, obtained as in Figure 3, are shown in the lower panel where the amount of iron-free IRP1 (darker bar) and iron-bound IRP1 (lighter bar) are compared. Data are representative of four independent experiments with similar results.

treatment caused a major shift to the B band with the complete disappearance of the C band (Figure 4, lane 3), H_2O_2 showed minor effects on IRP1 pattern, while iron supplementation caused a significant increase of the C band (Figure 4, lanes 4 and 5). Gel densitometry supported the indication of Figure 3 that Fe treatment induced an increase of total free IRP1.

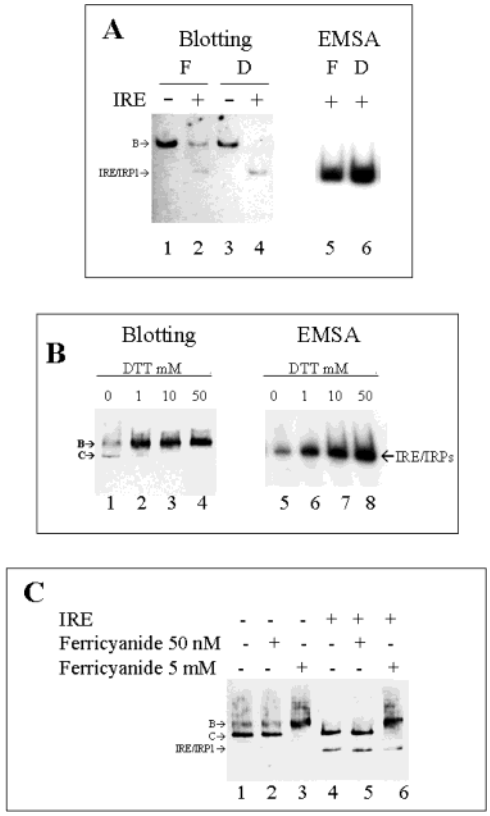

FIGURE 5: In vitro treatments of HeLa cell soluble extracts. (A) 10 μg of soluble extracts form HeLa cells treated with FAC or DFO, as in Figure 3, were incubated with 2% 2ME and, where indicated, 0.5 μL of unlabeled IRE probe was added (lanes 2 and 4), and samples run on nondenaturing 7.5% PAGE and blotted. In parallel, the same samples incubated with 2% 2ME, 100 000 cpm ^{32}P-labeled IRE probe was added and samples were analyzed by EMSA. (B) The soluble fraction of HeLa cells was incubated with increasing concentration of DTT and analyzed by blotting (10 μg) (lanes 1−4) and by EMSA (2 μg) (lanes 5−8). (C) 10 μg of HeLa soluble extract was incubated with 50 nM or 5 mM ferricyanide for 10 min at 25 °C and then with 0.5 μL of unlabeled IRE probe, where indicated. The samples were separated on nondenaturing 7.5% PAGE and blotted. Data are representative of two independent experiments with similar results.

Comparison of Blotting and EMSA. EMSA of cellular extracts treated with 2% 2ME showed a stronger signal in DFO than in FAC-treated cells (Figure 5A, lanes 5 and 6). The technique is considered to give an indication of total IRPs, but the result contrasted with blotting data showing an increase of total soluble IRP1 after FAC treatment (Figure 3). Therefore, we analyzed by blotting the samples after 2% 2ME reduction and incubation with unlabeled IRE probe. In the DFO-treated cells all IRP1 was shifted to IRE/IRP1 complex, while in the FAC-treated cells the shift was partial (Figure 5A, lanes 2 and 4), as in the untreated controls (Figure 2B, lanes 4 and 5). As a consequence, the amount of the complex was higher in the DFO-treated than in the FAC-treated cells, in agreement with the result obtained by EMSA. In addition, we observed that 2% 2ME treatment of control cells caused a >10-fold increase of the IRE/IRP1 complex revealed by blotting (Figure 2B, lanes 3 and 5) and only ~1.5−2-fold of the complex detected by EMSA (not shown). Part of the difference could be attributed to the presence of IRP2 that is detected by EMSA but is not affected by 2ME. However, IRP2 accounts for only about 30% of the total IRP binding activity in HeLa cells (Figure

2A), and thus also other factors should be considered, for example, the presence of 1 mM DTT in the EMSA incubation buffer. Indeed, we found that addition of 1 mM DTT before blotting increased the B band (Figure 5B, lane 2). Conversely, the omission of 1 mM DTT in the EMSA buffer decreased the signal of 2−3-fold (Figure 5B, lane 5). Ferricyanide at the concentration of 50 nM did not modify the intensity or mobility of band C (Figure 5C, lane 2), while at the concentration of 5 mM it caused a complete C → B shift (Figure 5C, lane 3). The results indicate that the [3Fe-4S] IRP1 produced by incubation with 50 nM ferricyanide (*26*) has the same mobility as the [4Fe-4S]−IRP1−aconitase, and are consistent with the evidence that high ferricyanide concentrations (e.g., 5 mM) disassemble IRP1 Fe/S clusters without increasing IRE-BP activity (Figure 5C, lane 6). We concluded that A and B bands represent the iron-free forms and the C band represents the iron-bound form of IRP1, independent from their IRE-BP or aconitase activities. Taken all together, these results show that EMSA overestimates the actual IRE-BP activity of IRP1 because of the partial activation by 1 mM DTT, commonly used to prepare cell extracts, and that it underestimates the total amount of IRP1 (after 2% ME reduction), because it does not detect the portion that does not bind IRE, which represents about 30% of cellular IRP1, except in iron-deprived cells. Therefore, the present results indicate that blotting is more accurate than EMSA in evaluating total IRP1 and its conformations.

Analysis of IRP1 in K562 Cells. We extended IRP1 blotting analysis to K562 cells, a cellular model extensively used for the study of the IRE−IRPs machinery. First, we evaluated total IRP1 in the soluble and precipitate fractions of the extracts. In the precipitate fraction IRP1 was present in low amounts in untreated cells and decreased even further after FAC treatment, while it increased substantially after DFO (∼8-fold) and H_2O_2 treatments (∼5-fold, Figure 6A). Gel densitometry analysis confirmed that the treatments did not modify the total amount of IRP1 but rather caused a shift between the two compartments. In K562 cells, a faint A band was also detected in addition to the B and C bands already observed in HeLa cells (Figure 6B). Band A (like band C) shifted to B after incubation of the samples with 2% 2ME- (not shown), and thus, by analogy with the results obtained with recombinant IRP1, we believe that it may represent a partially oxidized apo-IRP1. In the untreated cells, the proportion between iron-free form (represented by A and B bands) and the iron-bound form (band C) was similar to that observed in HeLa cells. Iron supplementation caused an increase of band C similar to that found in HeLa cells, whereas after DFO treatment the shift to B band was not as complete as it was in HeLa cells, and the change of IRP1 conformations was analogous to that caused by H_2O_2 treatment. The data obtained by densitometric analysis are summarized in Table 1.

IRP1 in Monocytes/Macrophages. Next, we analyzed IRP1 in human macrophages that were obtained by allowing freshly purified monocytes to differentiate in culture. Similarly to K562 cells, IRP1 in the precipitate fraction accounted for a minor proportion in the untreated macrophages, and it was only marginally affected by FAC treatment, while increased ∼3-fold after DFO and ∼2-fold after H_2O_2 treatment (Figure 7A). In the untreated cells, IRP1 in the soluble fraction was found in high proportion in the iron-free form. Treatment with DFO caused a shift of IRP1 to the B/A bands, similar to that found in HeLa cells, FAC had minor effects and H_2O_2 increased the C band (Figure 7B). The data obtained are summarized in Table 1.

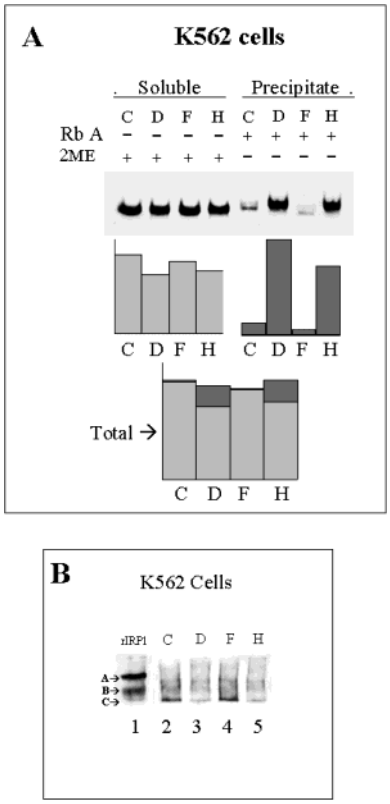

FIGURE 6: IRP1 in the soluble and precipitate fraction of K562 cells after iron chelation, supplementation or H_2O_2 treatment. K562 cells were treated as described in Figure 3 for HeLa cells. (A) The soluble fraction was incubated with 2% 2ME and the precipitate with RNase-A as in Figure 2. The samples (10 μg) were run on nondenaturing 6% PAGE, blotted with anti-IRP1 antibody, and densitometry data summarized as in Figure 3. (B) 10 μg of soluble extracts were analyzed on nondenaturing 7.5% PAGE and blotted with anti-IRP1 antibody. The arrows indicate the position of the A, B, and C bands. Densitometric values of the bands are shown under the electrophoretic patterns. The lower histograms represent the sum of the densitometric values of the soluble (lighter bar) and precipitate fraction (darker bar) obtained as described in Figure 3. Data are representative of three independent experiments with similar results.

IRP1 in Human Tissues. To verify the usefulness of the blotting technique at the study of IRP1 in tissues, we analyzed biopsy specimens from stomach and duodenum. Blotting of the soluble fraction treated with 2% 2ME showed a strong band with the mobility of B band and a minor faster-running band of uncertain identification (Figure 8A). Most IRP1 was found in the soluble fraction, and only trace amounts in the precipitate, RNase-A-treated, fraction (Figure 8A). In the soluble fraction, C band was predominant in both tissues, and all bands shifted to the B band after reduction with 2% 2ME, as expected (Figure 8B). No significant differences in the band pattern were found between stomach and duodenum. The weak faster band present in all samples apparently represents unrelated proteins with peroxidase activity.

Table 1: RNA-Bound and Iron-Free IRP1 in Cell Homogenates[a]

	RNA-bound[b]	fraction of RNA-bound[c]	bands A + B[d]	fraction of A + B[e]
		HeLa Cells		
control	1.0	0.11	1.0	0.43
DFO	3.5	0.52	1.9	~1
FAC	0.3	0.04	1.1	0.28
H_2O_2	2.2	0.38	0.7	0.39
		K562 Cells		
control	1.0	0.01	1.0	0.4
DFO	8.0	0.26	0.8	0.72
FAC	0.5	0.01	0.7	0.25
H_2O_2	5.8	0.18	0.6	0.75
		Macrophages		
control	1.0	0.003	1.0	0.6
DFO	3.3	0.008	1.4	~1
FAC	0.8	0.003	0.4	0.4
H_2O_2	2.3	0.002	0.8	0.5
		Stomach		
	n.d.	0.001	n.d.	0.3
		Duodenum		
	n.d.	0.0001	n.d.	0.2

[a] Densitometric data of IRP1 forms in cells and tissues extracts. [b] Ratio between the IRP1 in the RNAse-A-treated precipitate fraction of treated cells respect to the untreated control cells. [c] Ratio between the IRP1 in the RNAse-A-treated precipitate fraction respect to the total amount of IRP1 in the soluble and precipitate fractions. [d] Ratio between the iron-free IRP1 (bands A + B) in the soluble fraction of treated cells respect to the same of the untreated control cells. [e] Ratio between the iron-free IRP1 (bands A + B) respect to total IRP1 in the soluble fraction (bands A + B + C). Data from Figures 3, 4, 6, 7, and 8.

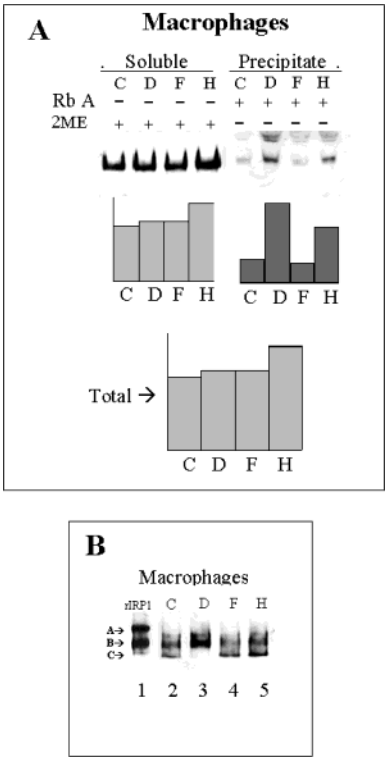

FIGURE 7: IRP1 in the soluble and precipitate fractions of macrophages after iron chelation, supplementation, or H_2O_2 treatment. To induce differentiation to macrophages, monocytes were maintained in culture for 7 days and then treated as described in Figure 3 for HeLa cells. The cellular extracts were analyzed as in Figure 6. (A) The soluble and precipitated fractions were analyzed on nondenaturing 6% PAGE. (B) Soluble fractions were analyzed on nondenaturing 7.5% PAGE. Densitometric values of the bands are shown under the electrophoretic patterns. The lower histograms represent the sum of the densitometric values of the soluble (lighter bar) and precipitate fraction (darker bar) obtained as described in Figure 3. Data are representative of two independent experiments with similar results.

DISCUSSION

The modifications of IRP1 conformation in cell extracts are normally evaluated by measuring either the IRE-BP or the aconitase activity, which are mutually exclusive. Blotting of IRP1 is a new assay, based on the different electrophoretic mobility of the iron-free and iron-bound forms, which allows the analysis of the IRP1 status at the level of protein conformation rather than activity and offers the possibility to investigate also the RNA-bound form, which is neglected by EMSA.

The Different IRP1 Forms Detected by Blotting. Blotting detected four forms of recombinant IRP1 with different mobilities. Two of them, A and B bands, were found in purified recombinant apo-IRP1. The slower A band was found also in K562 cells and macrophages, but not in HeLa cells and tissue extracts. It has IRE-BP activity comparable to that of B band, and it was partially converted into the faster B band by chemical reduction. Although the structure of this form is unknown, we assume that it is a partially oxidized apo-IRP1 form functionally similar to B band. The major form of apo-IRP1 was represented by band B, which is functionally heterogeneous, since a significant fraction of it does not have high affinity for IRE probe after 2% 2ME treatment. The inactive portion was undetectable in the untreated HeLa cell extracts (Figure 5A, lane 4), but was quantitatively important, about 30%, in rIRP1 (Figure 1B, lane 8) and in HeLa cell extracts chemically treated with 2% 2ME (Figure 2B, lane 5). The finding suggests that in vitro treatment of IRP1 with 2% 2ME, while disassembling the Fe/S cluster and activating IRE-BP activity, also partially damages IRP1 and impairs its capacity to bind IRE. This is in agreement with earlier data showing that the 2% 2ME-treated IRP1 is functionally different from the natural IRE-BP-active IRP1 (*26*). The practical consequence of this finding is that EMSA of 2% 2ME-treated extracts underestimates the total IRP1 protein, although this procedure is commonly used to evaluate total cellular IRP1.

Band C contained Fe/S-IRP1 and had aconitase activity. Its electrophoretic mobility was faster than that of apo-IRP1, consistent with a more compact conformation (*19*, *21*, *22*). Also this band was functionally heterogeneous, since it may as well contain the [3Fe-4S]-IRP1 with no aconitase activity. This was shown by the finding that treatment with 50 nM ferricyanide, which is known to inactivate aconitase activity (*26*), did not affect the amount or mobility of band C (Figure 5C). Thus, blotting of the soluble cellular extracts provides data on the conformational status of IRP1, which is not necessarily related to IRP1 functional status.

The fast electrophoretic mobility of the IRE−IRP1 complex is likely due to the strong negative charge of nucleic acid. The blotting signal of this band was weaker than that for A, B, and C bands, indicating that the antibodies had a lower affinity for IRP1 in this conformation. EMSA recognizes the complex with much higher sensitivity and thus it is more adequate to study IRE-BP activity. However, the capacity of blotting to recognize the various IRP1 conformations permitted to show that the presence of 1 mM DTT,

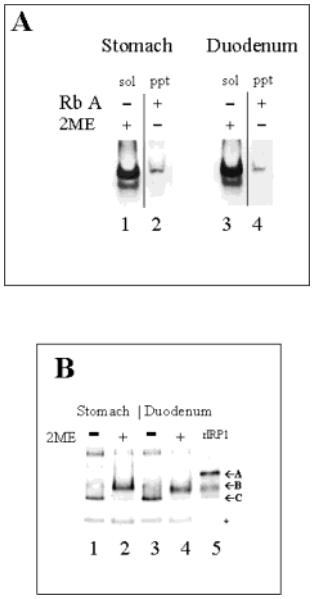

FIGURE 8: IRP1 in the soluble and precipitate fraction of stomach and duodenum tissues. Biopsy specimens of control subjects were taken from normal appearing mucosa of stomach or duodenum. (A) The soluble fraction (sol) was incubated with 2% 2ME and the precipitate fraction (ppt) with RNase-A as in Figure 2. Samples of 10 μg of total proteins were analyzed on nondenaturing 6% PAGE and blotted with anti-IRP1 antibody. (B) 10 μg of soluble extracts were left untreated or incubated with 2% 2ME, analyzed on nondenaturing 7.5% PAGE, and blotted with anti-IRP1 antibody. A minor band common to all samples, which probably represent proteins with peroxidase activity, is indicated by an asterisk. Data are representative of two independent analyses with similar results.

commonly used in EMSA buffer, is sufficient to activate IRE-BP activity in the cell extracts, and therefore it should be omitted for an accurate evaluation of the actual IRE-BP activity in a cell. The chemical reduction with 2% 2ME shifted all IRP1 to the B band, thus facilitating the evaluation of the total amount of the protein in the soluble fraction of the homogenates. The treatment increased the blotting signal 2−3-fold (Figure 2B). It is unlikely that this is due to a higher antibody affinity for the B band, since all the experiments with recombinant IRP1 showed the C and B to be equally recognized by the antibody. Thus, the causes of this increase are unclear, although we noticed that the treatment reduced the smear in the upper part of the gel often found in the unreduced samples.

Blotting was also used to analyze IRP1 in the precipitate fraction of HeLa cell extracts. We found that EMSA, detected just a minor proportion of the IRP1 in the fraction, and only after incubation with 2% 2ME. This supports the hypothesis that this fraction is enriched in mRNA-bound IRP1, and that it is liberated by in vitro RNase-A treatment. Furthermore, released IRP1 had the mobility of the iron-free B band, as expected. The amount of IRP1 freed after RNase-A treatment did not increase with longer incubations or with higher enzyme concentrations; therefore, we concluded that it represented all the RNA-bound IRP1. This fraction increased after cellular iron chelation and decreased after iron supplementation, as expected. Its proportion, while being within the range found previously in mouse fibroblasts by EMSA of high salt-treated extracts (*16*), was highly variable in the three cell lines we analyzed.

All together the major properties of blotting are the capacity to quantify and compare the relative amounts of free and RNA-bound IRP1 in cells extracts, and the capacity to distinguish between the iron-free and the iron-bound forms of soluble IRP1. Current model predicts that iron chelation would shift IRP1 to the iron-free form, and this in turn would bind RNA; therefore, the relative amounts of the iron-free and RNA-bound forms should be correlated to each other and to cellular iron availability.

IRP1 in K562 Cells and Macrophages. To verify this, we extended our analysis of IRP1 to other cellular models of physiological significance. We chose the erythroleukemic K562 cell line, a widely used model to study the regulation of iron metabolism, and monocytes/macrophages, cells which showed an unusual response to iron (*27*) and that are representative of the reticuloendothelial tissue, which has a major role in systemic iron metabolism. The cells were treated for iron chelation, supplementation and exposed to H_2O_2 under the same conditions so that blotting results are directly comparable. The results of densitometric analysis of blottings, summarized in Table 1, allowed us to evaluate free and RNA-bound IRP1, and to estimate the iron-free and iron-bound conformations in the soluble fractions. The table shows: (i) the relative amount of RNA-bound IRP1 referred to the control, and its proportion of the total detected IRP1 (free + RNA-bound), (ii) the relative amounts of the iron-free form (A + B bands), referred to the control and their proportion of relative to total soluble IRP1 (the sum of A + B + C bands). The data are in full agreement with the accepted model of IRP1 activity: iron chelation increased the RNA-bound and iron-free forms of IRP1 in the three cells types, and, conversely, iron supplementation decreased them. Inspection of the blotting patterns (Figures 3, 4, 6, and 7) and of the table shows that the most evident effect of manipulation of iron availability is the change of the amount (or fraction) of the RNA-bound form. This is particularly clear for iron supplementation, a treatment that has only subtle influence on the conformations of soluble IRP1 and whose effects are often undetectable by EMSA. This is consistent with strong upregulation of ferritin synthesis caused by iron-driven movement of IRP1 from the RNA-bound to the soluble compartment.

The total level of IRP1 and the general pattern of response to iron modifications were similar in the three cells types, but we observed important differences. HeLa cells had the highest proportion of RNA-bound IRP1: about 11% in the control and up to 52% after DFO treatment. In contrast, the corresponding values in K562 cells were 1 and 26%, and in macrophages were 0.3 and 0.8% (Figures 3, 6, and 7 and Table 1, column 3). In addition, the decrease of RNA-bound form caused by iron supplementation (Table 1, column 2) was lower in the macrophages (∼20%) than in HeLa and K562 cells (∼70 and 50%, respectively), while the increase after iron chelation was higher in K562 cells (∼8-fold) than in the other two cells (∼3−4-fold). Blotting of the soluble factions was of lower quality since the signals of A and B bands were often weak, and their quantification was somewhat difficult. However, the assay was able to provide semiquantitative data on the conformation of the IRP1 free forms, which should be related to IRP1 RNA-binding activity and that are detected by EMSA. Also in this case the general

pattern was the same in the three cell types, the iron-free form (bands A and B) increased with iron chelation and decreased with iron supplementation. After iron chelation, the C-band disappeared in HeLa and macrophages, but not in K562 cells. This was unexpected, and suggested that either K562 cells take up the chelator with lower efficiency or that their IRP1 recycling is different (in vitro incubation of the extract with DFO did not modify the blotting pattern, not shown). In addition, we observed that the iron-free forms were relatively more abundant in macrophages than in K562 and HeLa cells, in apparent contrast with the lower proportion of RNA-bound IRP1.

These data show previously undetected differences in IRP1 compartmentalization in the various cell types and under different conditions, which may be related to different levels of available target IREs and/or competition with IRP2. They may have a functional significance. The RNA-bound IRP1 should represent a pool to respond to iron excess, and the larger the pool, the stronger the response should be. In fact, HeLa cells which had a higher proportion of RNA-bound IRP1 responded to iron supplementation with a ~4-fold increase in ferritin synthesis (for both H and L chains), which was higher than that of K562 cells (~1.5- and ~2.2-fold for H and L ferritins, respectively, not shown). Thus, the high proportion of RNA-bound IRP1 seems to make HeLa cells better equipped to resist to iron excess. On the other hand, the capacity of IRP1 to move from the free to the RNA-bound compartment should be an index of the ability to respond to iron deficiency, and this was high in HeLa and K562 cells but not in macrophages. Accordingly, ferritin expression in the two cell lines was strongly suppressed down to 4−10% by DFO treatment and we predict that in macrophages the IRP1-dependent suppression of ferritin synthesis should be smaller. The findings suggest that IRP1 may play a minor role in the iron-dependent regulation, at least in macrophages and K562 cells. The function is probably mainly carried out by IRP2, which we found to be more abundant in K562 than HeLa cells (not shown) and that has been shown to be the major determinant of changes in ferritin expression in cytokine-treated mouse macrophages (*28*). This is also consistent with the observation that the iron-bound IRP1 form with putative aconitase activity was prevalent in all cells. It accounted for about 50% of total IRP1 and was only marginally modified by iron supplementation, reaching a maximum of 60−70% in the three cell types. It was virtually abolished by in vitro chelation with DFO, which, however, is probably a rather strong way to modify iron availability. The response to H_2O_2 was similar to that to DFO in the three cell types, as expected. Since the treatment with H_2O_2 was short, only 30 min, compared with the 18 h of iron chelation and supplementation, it appears that the shift from free to RNA-bound form may occur in a short period of time. In the macrophages, at variance with the other cells, H_2O_2 caused an increase in the iron-bound form that is presently unexplained.

Blotting of Tissue Extracts. Blotting can be applied also to study extracts from tissues. The ones available to us were from stomach and duodenum, the latter being the site of iron absorption. They differed from the cell extracts for having a 2−3-fold higher amount of IRP1 per unit of total protein (not shown) and a very low proportion of RNA-bound IRP1. In this respect, they are similar to the macrophages, primary cell lines that were maintained in culture for only one week. In addition, most soluble IRP1 was in the C band, indicating that in these tissues the very large majority of IRP1 is in the aconitase form. If this occurs in all other body tissues, then the IRP1 main function should be to regulate citrate metabolism, rather than iron homeostasis, as also suggested by the finding that IRP1 knockout mice do not show apparent abnormalities of iron homeostasis (*29*).

Conclusions. The major findings obtained by detecting most IRP1 conformations in tissues extracts with blotting can be summarized as follows: (a) EMSA under-evaluates the amount of total IRP1 and over-evaluates the actual IRE-BP activity of IRP1 when performed in the presence of 1 mM DTT; (b) the major effect of modifications in cellular iron availability is the shift between free and RNA-bound IRP1, which does not necessarily reflect the shift between iron-free and iron-bound forms of free IRP1; (c) the fraction of RNA-bound IRP1 is highly variable among different cells and is often a minor one; (d) the iron-bound aconitase IRP1 is by far the prevalent form in tissues. This latter point may offer an interpretation for a number of previous findings that were difficult to reconcile with the abundance of IRP1 in cell extracts that is commonly inferred by EMSA. Examples are represented by evidence that IRP1 was not required to maintain iron homeostasis in a mouse lymphocyte cell line (*30*), that nitric oxide-mediated IRP2 down-regulation, rather than the concomitant IRP1 activation, controls iron metabolism in cytokine-treated macrophages (*28*) and that the targeted deletion of IRP1 in mice did not cause any misregulation of iron handling (*29*).

ACKNOWLEDGMENT

We are grateful to Prof. Lukas K. Kuhn for the generous gift of plasmid pT7-His-hIRF.

REFERENCES

1. Cairo, G., and Pietrangelo, A. (2000) *Biochem J. 352*, 241−250.
2. Rouault, T., and Klausner, R. (1997) *Curr. Top. Cell Regul. 35*, 1−19.
3. Hentze, M. W., and Kuhn, L. C. (1996) *Proc. Natl. Acad. Sci. U.S.A. 93*, 8175−8182.
4. Hanson, E. S., and Leibold, E. A. (2002) in *Molecular and Cellular Iron Transport* (Templeton, D. M., Ed.) pp 207−235, M. Dekker, New York.
5. Kaptain, S., Downey, W. E., Tang, C., Philpott, C., Haile, D., Orloff, D. G., Harford, J. B., Rouault, T. A., and Klausner, R. D. (1991) *Proc. Natl. Acad. Sci. U.S.A. 88*, 10109−10113.
6. Kennedy, M. C., Mende-Mueller, L., Blondin, G. A., and Beinert, H. (1992) *Proc. Natl. Acad. Sci. U.S.A. 89*, 11730−11734.
7. Kaldy, P., Menotti, E., Moret, R., and Kuhn, L. C. (1999) *EMBO J. 18*, 6073−6083.
8. Gegout, V., Schlegl, J., Schlager, B., Hentze, M. W., Reinbolt, J., Ehresmann, B., Ehresmann, C., and Romby, P. (1999) *J. Biol. Chem. 274*, 15052−15058.
9. Pantopoulos, K., and Hentze, M. W. (1998) *Proc. Natl. Acad. Sci. U.S.A. 95*, 10559−10563.
10. Gehring, N. H., Hentze, M. W., and Pantopoulos, K. (1999) *J. Biol. Chem. 274*, 6219−6225.
11. Corsi, B., Levi, S., Cozzi, A., Corti, A., Altimare, D., Albertini, A., and Arosio, P. (1999) *FEBS Lett. 460*, 149−152.
12. Cairo, G., Tacchini, L., Pogliaghi, G., Anzon, E., Tomasi, A., and Bernelli-Zazzera, A. (1995) *J. Biol. Chem. 270*, 700−703.

13. Roy, C. N., Blemings, K. P., Deck, K. M., Davies, P. S., Anderson, E. L., Eisenstein, R. S., and Enns, C. A. (2002) *J. Cell. Physiol. 190*, 218−226.
14. Drapier, J. C., and Hibbs, J. B., Jr. (1996) *Methods Enzymol. 269*, 26−36.
15. Brown, N. M., Kennedy, M. C., Antholine, W. E., Eisenstein, R. S., and Walden, W. E. *J. Biol. Chem*. (2002) *J. Biol. Chem. 277*, 7246−7254.
16. Seiser, C., Posch, M., Thompson, N., and Kuhn, L. C. (1995) *J. Biol. Chem. 270*, 29400−29406.
17. Gray, N. K., Quick, S., Goossen, B., Constable, A., Hirling, H., Kuhn, L. C., and Hentze, M. W. (1993) *Eur. J. Biochem. 218*, 657−667.
18. Constable, A., Quick, S., Gray, N. K., and Hentze, M. W. (1992) *Proc. Natl. Acad. Sci. U.S.A. 89*, 4554−4558.
19. Brazzolotto, X., Timmins, P., Dupont, Y., and Moulis, J. M. (2002) *J. Biol. Chem. 277*, 11995−12000.
20. Brazzolotto, X., Gaillard, J., Pantopoulos, K., Hentze, M. W., and Moulis, J. M. (1999) *J. Biol. Chem. 274*, 21625−21630.
21. Schalinske, K. L., Anderson, S. A., Tuazon, P. T., Chen, O. S., Kennedy, M. C., and Eisenstein, R. S. (1997) *Biochemistry 36*, 3950−3958.
22. Gegout, V., Schlegl, J., Schlager, B., Hentze, M. W., Reinbolt, J., Ehresmann, B., Ehresmann, C., and Romby, P. (1999) *J. Biol. Chem. 274*, 15052−15058.
23. Cairo, G., Recalcati, S., Montosi, G., Castrusini, E., Conte, D., and Pietrangelo, A. (1997) *Blood 89*, 2546−2553.
24. Mullner, E. W., Neupert, B., and Kuhn, L. C. (1989) *Cell 58*, 373−382.
25. Selander, R. K., Caugant, D. A., Ochman, H., Musser, J. M., Gilmour, M. N., and Whittam, T. S. (1986) *Appl. Environ. Microbiol. 51*, 873−884.
26. Haile, D. J., Rouault, T. A., Harford, J. B., Kennedy, M. C., Blondin, G. A., Beinert, H., and Klausner, R. D. (1992) *Proc. Natl. Acad. Sci. U.S.A. 89*, 11735−11739.
27. Testa, U., Petrini, M., Quaranta, M. T., Pelosi-Testa, E., Mastroberardino, G., Campagna, A., Boccoli, G., Sargiacomo, M., Isacchi, G., Cozzi, A., et al. (1989) *J. Biol. Chem. 264*, 13181−13187.
28. Recalcati, S., Taramelli, D., Conte, D., and Cairo, G. (1998) *Blood. 91*, 1059−1066.
29. LaVaute, T., Smith, S., Cooperman, S., Iwai, K., Land, W., Meyron-Holtz, E., Drake, S. K., Miller, G., Abu-Asab, M., Tsokos, M., Switzer, R. 3rd, Grinberg, A., Love, P., Tresser, N., and Rouault, T. A. (2001) *Nat. Genet. 27*, 209−214.
30. Schalinske, K. L., Blemings, K. P., Steffen, D. W., Chen, O., and Eisenstein, R. S. (1997) *Proc. Natl. Acad. Sci. U.S.A. 94*, 10681−10686.

BI035386F